THE LIFE-TIME OF THERMAL PHONONS IN α-QUARTZ

By

ASHOK K. KOCHHAR, M.Sc.

A Thesis

Submitted to the School of Graduate Studies

in Partial Fulfilment of the Requirements

for the Degree

Master of Science

McMaster University

March 1979

THE LIFE-TIME OF THERMAL PHONONS IN α-QUARTZ

MASTER OF SCIENCE (1979) McMASTER UNIVERSITY
(Physics) Hamilton, Ontario

TITLE: The Lifetime of Thermal Phonons in α-Quartz

AUTHOR: Ashok K. Kochhar, M.Sc. University of Delhi, India

SUPERVISOR: Professor D. Walton

NUMBER OF PAGES: vi, 57

Abstract

The attenuation of thermal phonons and acoustically generated phonons at different power levels are compared in α-quartz. The average attenuation at 1.67 GHz at room temperature was 27.3 db/cm ± 2.7% and at a frequency of 1.856 GHz, it was 32.5 db/cm ± 2.1%. Woodruff and Ehrenreich's theory was used to calculate the lifetime of thermal phonons from acoustic attenuation data. The relaxation time for thermal phonons at 300°K was found to be 8.34×10^{-12} sec.

ACKNOWLEDGMENTS

I wish to express my thanks to my supervisor, Professor D. Walton, for his advice and assistance throughout the course of this work. I also extend my thanks to Dr. Frank Lin for his valuable assistance with many technical problems. A special thanks is also due to Mr. Robert Donders and Mr. Paul Waterhouse for their cooperation during the course of this work. My sincere thanks to Mrs. Helen Kennelly for doing a wonderful job of typing the thesis.

This work was made possible through the financial support of the McMaster Physics Department and the National Research Council of Canada.

I dedicate this work to my parents and my wife.

TABLE OF CONTENTS

LIST OF FIGURES

CHAPTER 1

INTRODUCTION AND THEORY

Woodruff and Ehrenreich [47] extending a theory of Akhieser [1] have derived a theoretical expression for the attenuation of low frequency sound waves in insulators which they have compared with the experiments conducted by Bömmel and Dransfeld [8]. Landau and Rumer [25] provide a quantum mechanical treatment limited to $\Omega\tau > 1$ where Ω is the frequency of the sound wave and τ is the mean time between collisions for thermal phonons. Their theory is not valid for the case $\Omega\tau \leq 1$.

Akhieser's [1] mechanism for absorption of energy arises partly from heat flow and partly from viscous damping. His calculation of the viscous damping contribution to sound absorption is based upon the idea that the sound wave modulates the elastic properties and hence the thermal phonon frequencies of the medium through which it propagates. The modulated phonons are no longer in thermal equilibrium but relax towards local thermal equilibrium via phonon-phonon collisions, caused by anharmonic interaction.

Woodruff and Ehrenreich [47] assume that the sound wave varies the frequencies of the thermal phonons adiabatically, and a complete Boltzmann equation is set up to

determine the response of the thermal phonon distribution to this disturbance. As the driving term has an explicit time variation, the collision time is written in terms of relaxation times for normal phonon-phonon collision (N-processes) and all other processes (U-process) both of which tend to relax the distribution function to an equilibrium distribution which is characteristic of a local temperature T', and in the case of the N processes is shifted in phonon wave number space away from the origin. In fact the temperature T' arises here because the perturbation of the distribution function by the sound wave (of wave length Λ) driving the system depends upon the polarization of the thermal phonons. This leads to a local relaxation of these phonons, by a process having no analog in the theory of thermal conductivity of insulators, towards a Planck distribution for which the phonons in all branches are at a common temperature T' different from the ambient temperature of crystal.

First the distribution function $N(\vec{q},\vec{r},t)$ for the population of thermal phonons in a sample of unit volume is determined. $N(\vec{q},\vec{r},t)$ is the number of phonons of mode $\vec{q}$ at position $\vec{r}$ and time t. The driving sound wave is represented as a traveling plane wave of elastic displacement of the form

$$u_0 \cos[i(\vec{\sigma}.\vec{r}-\Omega t)]$$

where u_0 is the amplitude and $\vec{\sigma}$ and Ω are wave vector and

frequency of the wave respectively. This approach is valid so long as $\sigma < q_{th}$, the wave number of the most abundant thermal phonon excitation, or neglecting the dispersion in the velocity of sound so long as

$$\Omega < k_B T/\hbar$$

where k_B is Boltzmann constant and $\hbar$ being Planck's constant.

If we assume the direction of sound propagation of wavelength Λ is in the z-axis, then the Hamiltonian for a single phonon q at position z at time t, under the influence of the externally applied sound wave is

$$H(\vec{q},z,t) = H_0(\vec{q}) + H_1(\vec{q},z,t) = \hbar\omega(\vec{q},z,t) \qquad (I.1)$$

where

$$H_0(\vec{q}) = \hbar\omega_0(\vec{q})$$

and

$$H_1 = a(\vec{q};\vec{\sigma},\vec{u}_0)H_0(\vec{q})\exp[i(\sigma z-\Omega t)]$$

or

$$H_1 = \psi(\vec{q};\vec{\sigma},\vec{u}_0)\exp[i(\sigma z-\Omega t)] \qquad (I.2)$$

Thus the perturbed frequency ω is given by

$$\omega(\vec{q},z,t) = \omega_0(\vec{q})\ \{1 + a(\vec{q};\vec{\sigma},\vec{u}_0)\exp[i(\sigma z-\Omega t)\} \qquad (I.3)$$

where $\omega_0(\vec{q})$ is the frequency of a phonon of mode $\vec{q}$ in the unstrained crystal and $a(\vec{q},\vec{\sigma},\vec{u}_0)$ is a coefficient depending in a complicated way on $\vec{q}$ and $\vec{\sigma}$ and linearly on $\vec{u}_0$ for small amplitudes.

Now we should distinguish three different distribution functions:

(a) The thermal equilibrium distribution at temperature T.

$$N_0(\omega_0) = \frac{1}{\left[\exp\left(\frac{\hbar\omega_0}{k_B T}\right) - 1\right]} \tag{I.4}$$

(b) the local equilibrium distribution $N_0(\omega)$ corresponding to the perturbed frequencies ω.

(c) And finally the perturbed distribution

$$N(\vec{q};z,t)$$

Since in practice, the attenuation is pretty small, we can write, to first order, the perturbed distribution function in terms of the total equilibrium distribution as

$$N(\vec{q},z,t) = N_0(\omega) - \frac{N_0'}{k_B T}\,\phi(\vec{q};\vec{\sigma},u_0) \times \exp[i(\sigma z - \Omega t)] \tag{I.5}$$

where

$$N_0' \equiv \frac{dN_0(\omega_0)}{d\left(\frac{\hbar\omega_0}{k_B T}\right)}$$

and $\phi(\vec{q};\vec{\sigma},u_0)$ being the wave function with usual notations.

If we relate the perturbed distribution to the thermal equilibrium distribution in first order

$$N(\vec{q},z,t) = N_0(\omega_0) + N_1. \tag{I.6}$$

The Boltzmann transport equation can be written as

$$\left(\frac{\partial N}{\partial t}\right)_{coll} = \frac{\partial N}{\partial t} + \frac{1}{\hbar}\sum_{i=1}^{3}\left(\frac{\partial N}{\partial r_i}\frac{\partial H}{\partial q_i} - \frac{\partial N}{\partial q_i}\frac{\partial H}{\partial r_i}\right) \qquad (I.7)$$

where r_i are the position coordinates and the $\hbar q_i$ the momentum coordinates of the phonons, here considered as classical particles.

The approximation to the collision term is constructed. We know that the scattering processes fall into two classes:

(i) N-processes which conserve the phonon wave vector.

(ii) U-processes which do not conserve the phonon wave vector.

And $\tau_N(\vec{q})$ and $\tau_U(\vec{q})$ are the respective relaxation times. Now both types of processes produce relaxation towards Planck distributions which are characterized by an effective temperature

$$T'(z,t) \equiv T + \Delta T \exp[i(\sigma z - \Omega t)] \qquad (I.8)$$

where $T'(z,t)$ is the temperature which would ultimately be obtained in a small region around a point, if at time t, this region were isolated from the remainder of the solid but maintained in the state of strain existing in it at that time. And also the total relaxation time is given as

$$\frac{1}{\tau(\vec{q})} = \frac{1}{\tau_N(\vec{q})} + \frac{1}{\tau_U(\vec{q})} . \qquad (I.9)$$

Now since the average rate at which energy is removed from the sound wave is equal in the steady state to the average rate Q at which energy is transferred from the phonon system to the

heat bath

$$Q = - \sum_{q,j} \langle H(\frac{\partial N}{\partial t})_{coll} \rangle \quad . \tag{I.10}$$

And if equation (I.7) is substituted in the above equation and making relevant approximations; we get

$$Q = \frac{V}{16\pi^3} \sum_j \int d^3q \; Re\{N_1^* \frac{\partial H_1}{\partial t}\} \tag{I.11}$$

and the attenuation (Γ) is given by

$$\Gamma = Q/cW \tag{I.12}$$

where W is the energy density of the sound wave and c being the average velocity of sound wave in the solid.

$$W = \rho\Omega^2 u_0^2/2 \tag{I.13}$$

where ρ is the mass density, and

$$(\frac{3}{c^3}) = (\frac{1}{c_\ell^3}) + (\frac{2}{c_t^3}) \tag{I.14}$$

where c_ℓ and c_t are longitudinal and transverse velocity of sound in the media. If $W_0(\vec{q},j)$, $\tau_N(\vec{q},j)$, $\tau_u(\vec{q},j)$ etc. are known, we can determine Q. Since the knowledge of these functions is incomplete for most materials, thus the value of Q is found in the limiting cases when the solid can be represented by the Debye model for which

$$w(\vec{q},j) = c\vec{q} \quad . \tag{I.15}$$

Also τ_N and τ_U are supposed to be independent of $\vec{q}$. And we finally find for $\Omega\tau << 1$

$$\Gamma = \frac{C_v T \nu^2 \Omega^2 \tau}{3\rho c^3} \qquad (I.16)$$

where C_v is the total lattice specific heat of the solid and ν is a Grüneisen constant (see Appendix III).

If the thermal conductivity is

$$K = \frac{1}{3} C_v c^2 \tau \qquad (I.17)$$

then

$$\Gamma = \frac{\nu^2 \Omega^2 TK}{\rho c^5} \quad . \qquad (I.18)$$

At temperatures greater than Debye temperature of the solid, $K \propto \frac{1}{T}$. Thus KT and hence Γ became independent of temperature.

On the other hand for $\Omega\tau >> 1$, we get

$$\Gamma = \frac{\pi \nu^2 \Omega C_v T}{4\rho c^3} \quad . \qquad (I.19)$$

Equation (I.19) shows that Γ is independent of τ and has the same dependence upon Ω and T as that arrived at by Landau and Rumer [25] in their quantum mechanical treatment of the case $\Omega\tau > 1$. Woodruff and Ehrenreich [47] also discuss the case where $\Delta T = 0$ and $\Lambda = 0$ and this leads to the result

$$\Gamma = \frac{3\nu^2 \Omega^2 TK}{\rho c^5} \quad \frac{\tan^{-1}(2\Omega\tau)}{2\Omega\tau} \quad . \qquad (I.20)$$

Therefore for $\Omega\tau << 1$, Γ in equation (I.20) is three times the value that is given by equation (I.18). Γ is considerably smaller when ΔT is considered than when ΔT is neglected because for finite ΔT, the distribution function does not have as far to relax. This results in smaller collision terms and hence smaller attenuation. Equations (I.18) and (I.20) suggest that the low-power attenuation is three times more than the high-power one for the same frequency in the $\Omega\tau << 1$ range.

Thus the task before us was to decide which of these expressions best agreed with experiment. In the case of high power sound wave, a large ΔT would be expected. Therefore we study the attenuation of thermal phonons and acoustically generated phonons at different power levels and subsequently compare the two values.

CHAPTER II

(a) Description of the Experiment

By measuring the intensity of light scattered from a sound wave, at different positions along the crystal axis, it should be possible to measure its attenuation.

The material used for the acusto-optical experiment was a single crystal of α-quartz. Quartz was used as a piezo-electric transducer and propagating material on account of its mechanical properties and for the manner in which it can be cut and polished to very close tolerances. Also quartz is one of the materials for which extensive information is available concerning elastic and acoustic properties. We employed an X-cut, right circular cylinder with two Z polished faces. Its dimensions were 6×50 mm as shown in figure 1.

It is well known that acoustic waves in transparent materials can be used to scatter light. As a result, a great deal can be learned about the energy distribution in the acoustic beam by studying the angular and positional dependence of the optical-acoustic interaction. The sound column is injected

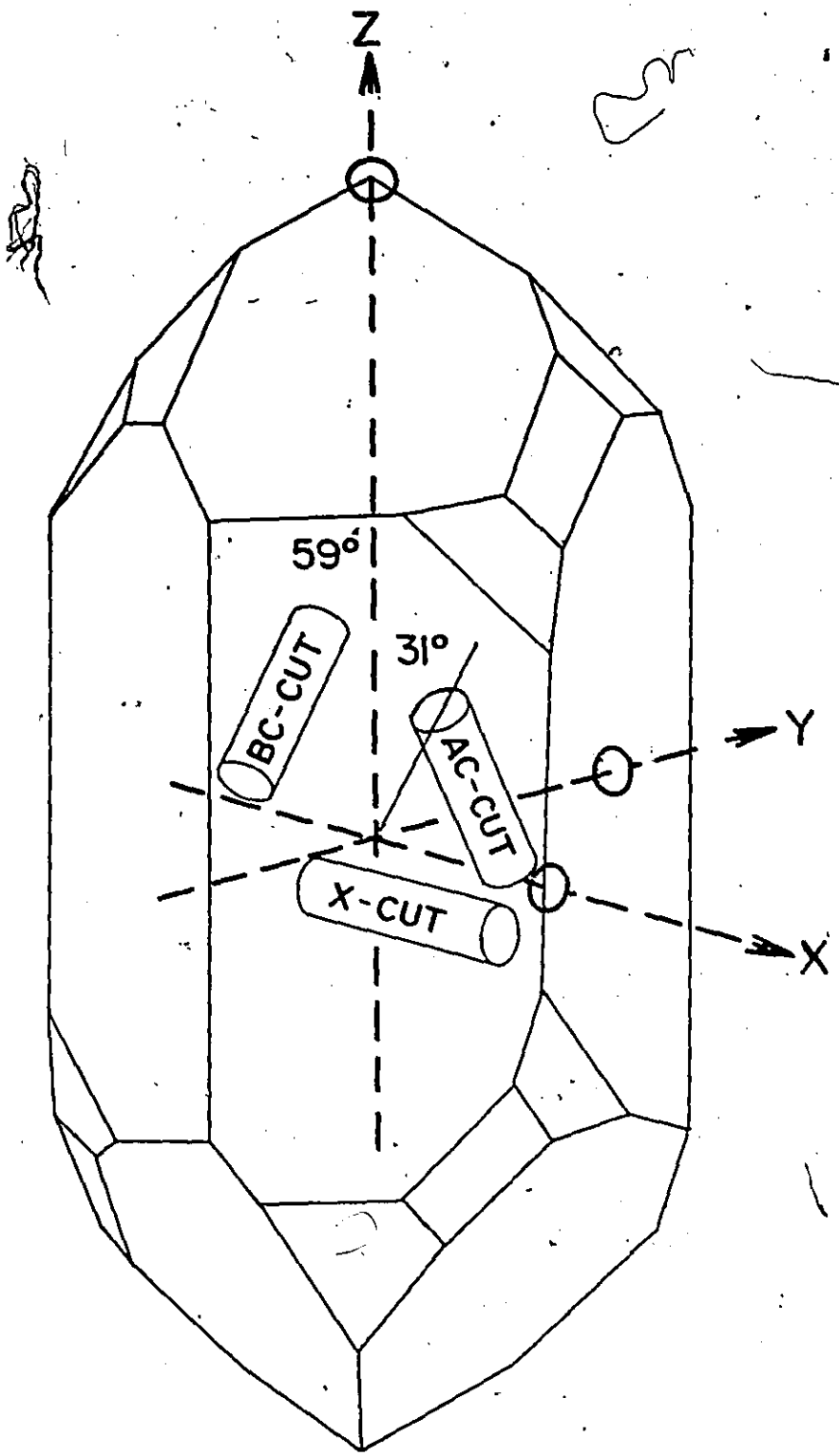

Fig. 2.1

Quartz cuts used as microwave ultrasonic transducers

piezo-electrically in the x direction by inserting one end of the quartz single crystal into a re-entrant microwave cavity. The compressions and rare-factions of the longitudinal acoustic wave act like a diffraction grating. Rytov [38] has shown that the phenomenon of diffraction of light by ultrasonic waves differs little from diffraction of light by a one-dimensional grating until

$$\lambda \ell / \Lambda^2 \quad . \qquad \text{(II.1)}$$

(λ, Λ - wavelength of light and sound, ℓ - length of path of light) becomes much smaller than unity. With decrease in Λ when the expression (II.1) becomes greater than unity, the three dimensional character of the ultrasonic lattice is manifested in selective (Bragg) reflection of light. The intensity of light diffracted at an angle ϕ to the incident light will be maximum, if the angle θ between the incident light and the plane of the sound wave front satisfies the condition

$$\sin\theta = \frac{1}{2} \frac{\vec{K}}{\vec{k}} \quad . \qquad \text{(II.2)}$$

The Bragg angle, which represents the conditions for momentum conservation to occur during the scattering process, for small θ, the equation (II.2) becomes

$$\theta = \frac{1}{2} \frac{\lambda}{\Lambda} = \frac{\phi}{2} \quad . \qquad \text{(II.3)}$$

In equation (II.2) $\vec{K}$ and $\vec{k}$ are the propagation constants (or wave vectors) of the incident sound and light beams respec-

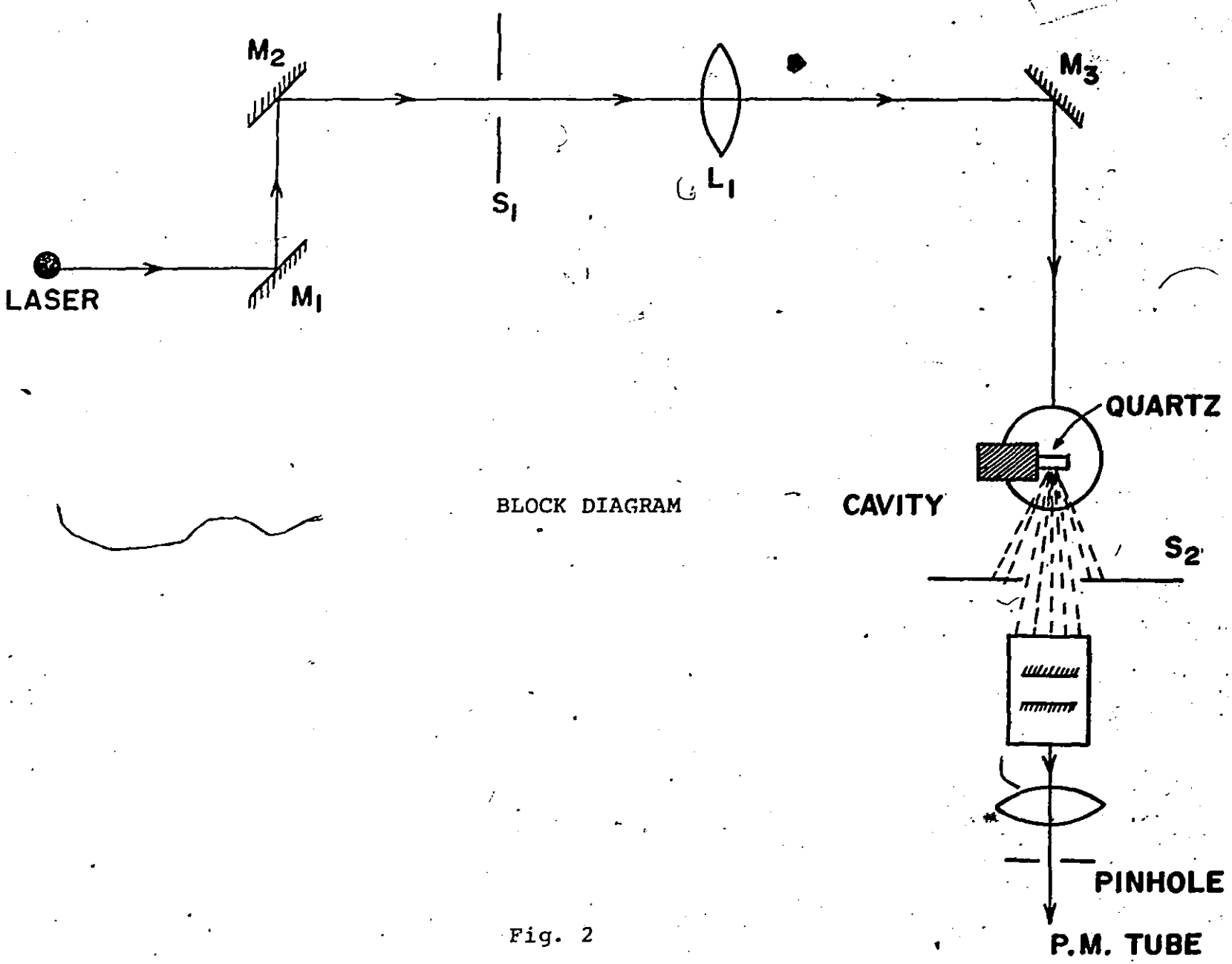

BLOCK DIAGRAM

Fig. 2

tively. Because the sound wave is attenuated, the intensity will decrease with distance from the end of the crystal in the cavity.

In our set up, the angle of incidence was determined by the above equations. Light of wavelength 4880 Å or 5145 Å from a laser passes through a focusing lens L_1 which focuses the beam and makes it incident at the Bragg angle, to be scattered by the sound column. After an iris, to limit the stray light, the scattered beam passes through a single-pass Fabry Perot interferometer (Appendix A2). The light is finally detected by a photomultiplier tube. A lens between Fabry-Perot and photomultiplier tube is used to focus the scattered light on the PM. The FP was used for qualitative analysis only.

The sides of the crystal were ground and polished flat to allow passage of the light in the desired direction. And for the generation of acoustic waves, both ends of the crystal were flat to $\lambda/10$ of the wave length and mutually parallel within 10 seconds of arc.

The optics of the system were first aligned without the crystal. Then the crystal, inserted into the re-entrant cavity (Appendix A1) was placed on a turntable, which was already adjusted to the calculated scattering angle. The data was collected and analyzed by a Nova-mini computer. Individual sets of data were obtained at different values of acoustic power. For a given power, various counts were taken,

along the whole length of the crystal in the x direction. The number of counts was quite high near the re-entrant cavity end; and they became progressively smaller going away from the re-entrant cavity end.

In order to eliminate the background counts, we collected the data twice at the same point in the crystal, once with the microwave generator 'on' and then 'off'. A typical set of data collected is shown in tables I and II. We did the experiment first with the help of a count meter but later with the Fabry-Perot interferometer. The output was displayed on an oscilloscope and recorded on an X-Y chart recorder.

We observed that the attenuation of hypersonic waves in quartz is dependent upon the square of the frequency of the acoustic wave. We found that average attenuation constant at 1.67 GHz frequency, was 27.3 db/cm ± 2.7% and at 1.856 GHz, it was 32.5 db/cm ± 2.1%. We were unable to find the attenuation constant at 3.456 GHz (at room temperature) because we could not detect the signal. The reason for this is that the attenuation at this frequency is quite high and therefore makes it quite difficult to see a signal, however, one could easily detect a signal in the low frequency region. The elastic and phonon peaks at different powers are shown in figure 2.4.

BLOCK DIAGRAM

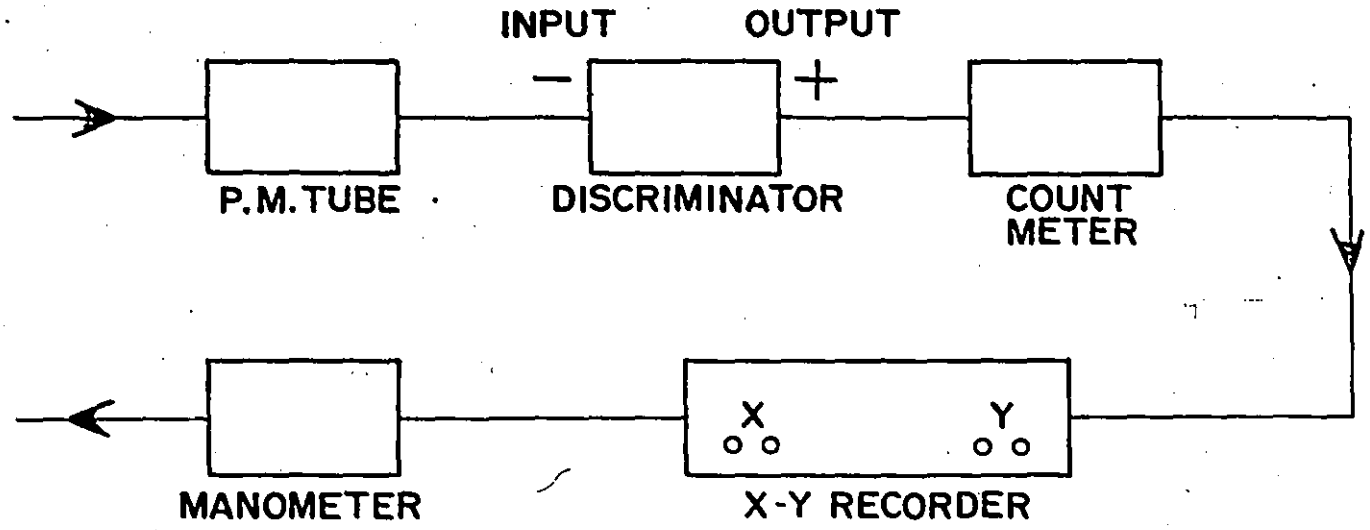

Fig. 2.3

Calculation of the Scattering Angle

(i) $\lambda = 4880\ \mathring{A}$ $\qquad \Lambda = \dfrac{5.78\times10^{5}}{1.67\times10^{9}}$ cm

$$\sin\theta = \frac{1}{2}\frac{\lambda}{\Lambda}$$

$$\sin\theta = \frac{1}{2}\frac{4880\times10^{-8}\times1.67\times10^{9}}{5.78\times10^{5}}$$

$$\theta = 4.04°$$

(b) $\Lambda = 5.78\times10^{5}/1.856\times10^{9}$ cm $\quad \theta = 4.49°$

(ii) $\lambda = 5145\ \mathring{A}$ $\qquad \Lambda = \dfrac{5.78\times10^{5}}{1.67\times10^{9}}$ cm

$$\sin\theta = \frac{1}{2}\frac{5145\times10^{-8}\times1.67\times10^{9}}{5.78\times10^{5}}$$

$$\theta = 4.26°$$

(b) $\Lambda = \dfrac{5.78\times10^{5}}{1.856\times10^{9}}$ cm $\qquad \theta = 4.73°$

Explanation of Variables from Tables I and II

(a) Counts is the actual number of counts due to the signal.

(b) % difference is the RMS differences with respect to the mean fit curve.

(c) Set position refers to the various points across the crystal.

(d) Total is the total number of counts due to both signal and background.

(e) ATC stands for attenuation constant and the values are in millimeters.

Note: All of the counts are in multiples of one thousand.

Table I

Typical data for 1.67 GHz
(at room temperature)

POWER IS 3.24

	% Difference	Position	Counts	Log (Count)
1	2.02775	95	33.8266	3.52125
2	-4.80222	94	24.0663	3.18081
3	-1.45133	93	18.9965	2.94425
4	1.69982	92	14.948	2.70458
5	.955142	91	11.3144	2.42608
6	7.07012	90	9.1498	2.21373
7	.887466	89	6.5739	1.88311
8	2.15539	88	5.0756	1.62444
9	-16.1654	87	3.159	1.5026

	% Difference	Position	Counts	Log (Count)
1	2.06392	95	33.8266	3.52125
2	-4.931	94	24.0663	3.18081
3	-1.75364	93	18.9965	2.94425
4	1.21478	92	14.948	2.70458
5	.301106	91	11.3144	2.42608
6	6.19437	90	9.1498	2.21373
7	-.109003	89	6.5739	1.88311
8	.973258	88	5.0756	1.62444

	% Difference	Position	Counts	Log (Count)
1	1.86601	95	33.8266	3.52125
2	-4.76094	94	24.0663	3.18081
3	-1.20922	93	18.9965	2.94425
4	2.15527	92	14.948	2.70458
5	1.61176	91	11.3144	2.42608
7	1.95424	89	6.5739	1.88311
8	3.44379	88	5.0756	1.62444

MFP = 3.66076 +- 2.68164 % RMS Deviation = 2.68681 %

*The computer eliminates the points which may have large errors.

Table II

Typical data for 1.856 GHz
(at room temperature)

```
RUN

No. of data pts., voltage, and no. of iterations
? 8? 1? 2500RMS Weight factor = ? 2
Set position and input 1
? 1 set position and input 1
? 2 set position and input 1
? 3 set position and input 1
? 4 set position and input 1
? 5 set position and input 1
? 6 set position and input 1
? 7 set position and input 1
? 8 set position and input 1
? 9
Power is 1
```

Total	% Difference	Position	Counts	Log (Cnts.)
40.8224	-1.17272	1	25.5344	3.24002
23.2688	3.50917	2	19.3128	2.96077
22.1348	-3.83569	3	12.9568	2.56162
39.8436	3.62041	4	10.082	2.31075
24.756	-1.84702	5	6.8964	1.931
67.7684	-4.30906	6	4.8552	1.58005
55.7142	-1.52801	7	3.608	1.28315
44.4944	-1.311	8	2.6112	.959809

```
Input 1 if recycle the fitting routine
? 2
ATC = -3.07177  +--2.10926 %  RMS Deviation = 2.90565 %

Y9 = 0
```

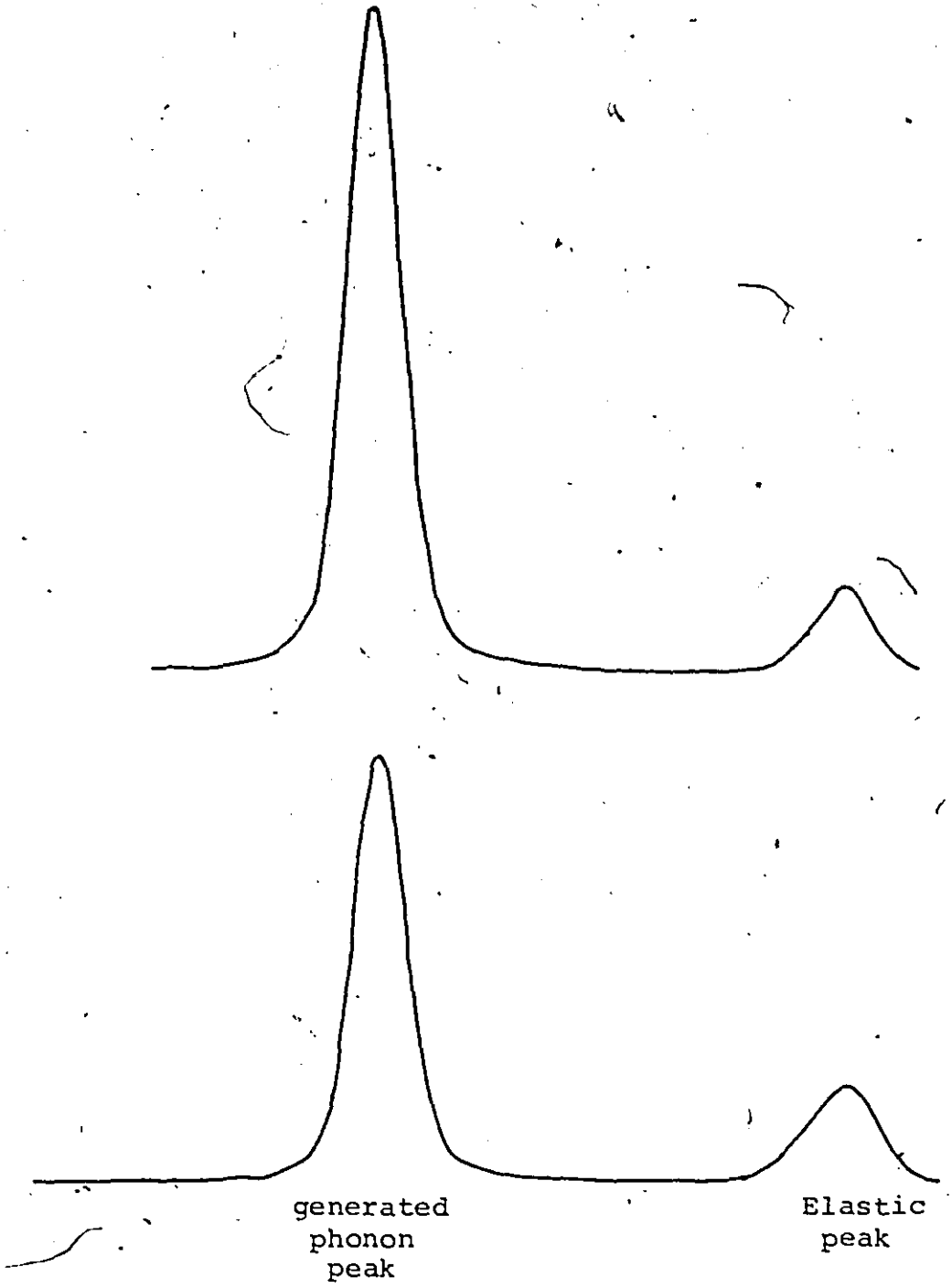

Fig. 2.4

Peaks at different powers

Table III

Various Constants of Quartz:- (α-cut)

density	=	2.652 gm/cc
(X-cut) longitudinal velocity	=	5.78×10^5 cm/sec
slow transverse velocity	=	3.3×10^5 cm/sec
fast transverse velocity	=	5.1×10^5 cm/sec
Debye temperature	=	563°K
C_v	=	(ref. Lord and Morrow [25A]
No. of atoms/unit cell	=	9

For various elastic constants, please refer to Appendix III.

CHAPTER III

CONCLUSION AND DISCUSSION

The average attenuation at 1.67 GHz for the room temperature was found to be 27.3 db/cm ± 2.7% and at a frequency of 1.856 GHz, it was 32.5 db/cm ± 2.1%. Assuming a frequency squared (Ω^2) behaviour and comparing these values to those obtained by other investigators [24], [41], [8], [16] etc. at different frequencies, we find that our measured values are a little bit high. One point to be noted is that so far most of the reported values at other frequencies have been obtained with the pulse-echo techniques. Even for the same frequencies, the measured values reported by different authors may differ by 20-25%. This can clearly be seen in figure 3.1. The possible error may be in the use of the technique itself. In order to get proper echoes, the ends of the crystal should be highly parallel, may be within 0.1-0.25 λ_0, and if it is not so, the measured attenuation can be quite erroneous. Stewart and Stewart [41] emphasize this point . They showed that at 3.2 GHz, if crystal plane-parallel is 0.25 λ_0, the attenuation is 4±0.4 Np/cm (1 Np ≡ 8.68 db), and if the crystal plane-parallel is 1 λ_0, the attenuation is 6±0.4 Np/cm.

Bömmel and Dransfeld [8] have made extensive measurements on quartz for the limiting case of $\Omega\tau << 1$; however their values seem to be on the lower side. Finally it should be noted that the practical detection sensitivity limits the pulse-echo method to attenuation of less than $\sim$ 10 db/cm.

The theory of sound absorption in solids involves the scattering of thermal phonons which are characterized by a relaxation time τ. If the hypersound has frequency Ω, the condition $\Omega\tau \simeq 1$ separates two limiting cases for the older theories. This condition is fulfilled for frequencies $\sim$ 3 GHz at room temperature.

The values which we obtained in the case of two frequencies were for a wide range of powers in the milliwatt range. The attenuation for each frequency at different powers was found to be of constant value within experimental errors.

Let us now review the theory of sound absorption in solids to compare different theories. Bömmel and Dransfeld [8] and Woodruff and Ehrenreich [47], as outlined previously, developed theories based upon Akhieser's mechanisms [1] of viscous damping. Nava et.al. [32] showed that the thermal phonons are simultaneously amplitude and frequency modulated. Bömmel and Dransfeld [8] neglected the velocity of the thermal phonons whereas Woodruff and Ehrenreich [47] included velocity but assumed it to be dispersionless. Maris [28] incorporated phonon dispersion into the $\Omega\tau >> 1$ perturbation limit first

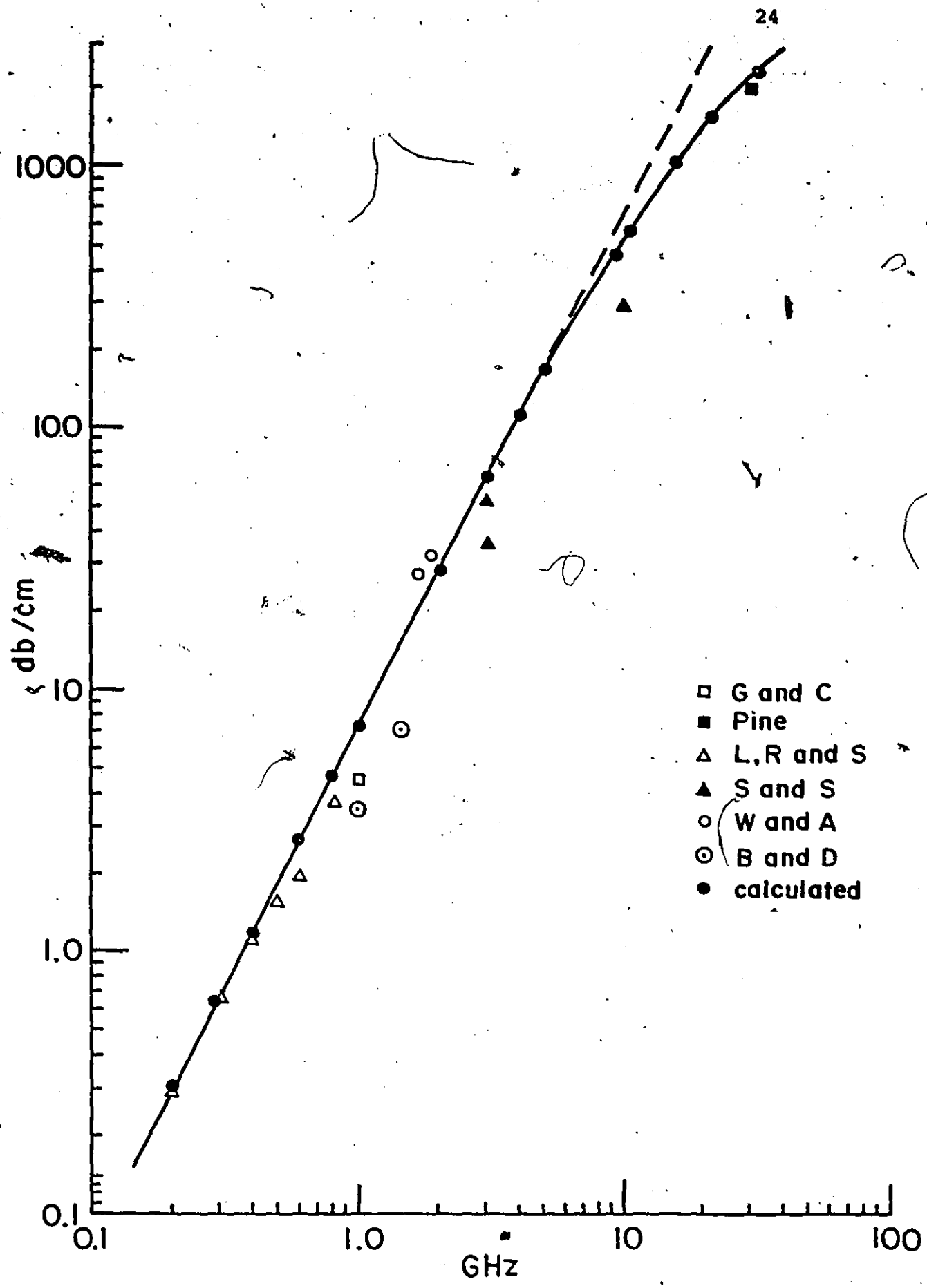
1000
100
10
1.0
0.1
db/cm
0.1
1.0
10
100
GHz
G and C
Pine
L, R and S
S and S
W and A
B and D
calculated

Fig. 3.1

studied by Landau and Rumer [25]. He applied his result to his measurements on quartz which were not, however, all taken with $\Omega\tau >> 1$ satisfied. Simons [45] gave a first order quantum mechanical perturbation theory valid for all $\Omega\tau$ in a dispersionless medium. But it was Kwok [18] who included the effect of dispersion and the full range of $\Omega\tau$ for a complete formulation. All the previous results are easily derived from Kwok's theory as special cases. Kwok [18] employed a Green's function technique of many body theory to obtain a general expression for phonon damping. However the approximations necessary to make Kwok's theory usable reduce his expression to that of Woodruff and Ehrenreich. Using the relationship between a line width and attenuation constant

$$\Gamma = \pi\delta\nu = \alpha v_\ell \qquad \text{(III.1)}$$

where $\delta\nu$ is the full width at half maximum [FWHM] or the linewidth and α is the attenuation constant. The different experimental values reported by the various authors were drawn on a log-log curve as shown in figure 3.1, along with our measured values. We then fit Woodruff and Ehrenreich's expression to the data with the lifetime of thermal phonons left as an adjustable parameter.

$$\Gamma = \frac{\nu^2 \Omega C_v T}{2\rho v_\ell^3} \tan^{-1} 2\Omega\tau \ . \qquad \text{(III.2)}$$

The value of the Grüneisen constant ν, which was used

was 0.708. A detailed discussion of the calculation of this parameter is given in Appendix A-III, where the values of all the Grüneisen numbers in the respective modes can be calculated from the third-order elastic constants. In fact Woodruff and Ehrenreich [47] treat ν as an adjustable parameter. The Grüneisen constant calculated by us was based upon Brügger's [11] formulation for rhombohedral crystals. The calculated value is fairly close to the measured value of 0.733. This measurement of ν was based upon the experimental determination of thermal expansion coefficients by Lewis [21].

The specific heat of α-quartz at different temperatures has been measured by Lord and Morrow [25A]. The variation of values with temperature is not that great. In the case of simple crystals, the value of specific heat is given by an expression which assumes that there is one atom per unit cell. In the case of complex lattices, which include N atoms in a unit cell instead of one, the specific heat in the expression for the attenuation must be modified. The specific heat required is that for a monoatomic lattice. Therefore, the measured heat capacity is

$$C_v' = C_v/N^{1/3} \quad . \qquad \text{(III.3)}$$

In the case of α-quartz, there are 9 atoms per unit cell, hence our value of the specific heat is the measured value multiplied by a factor of $N^{1/3} = 2.08$. The line shown in

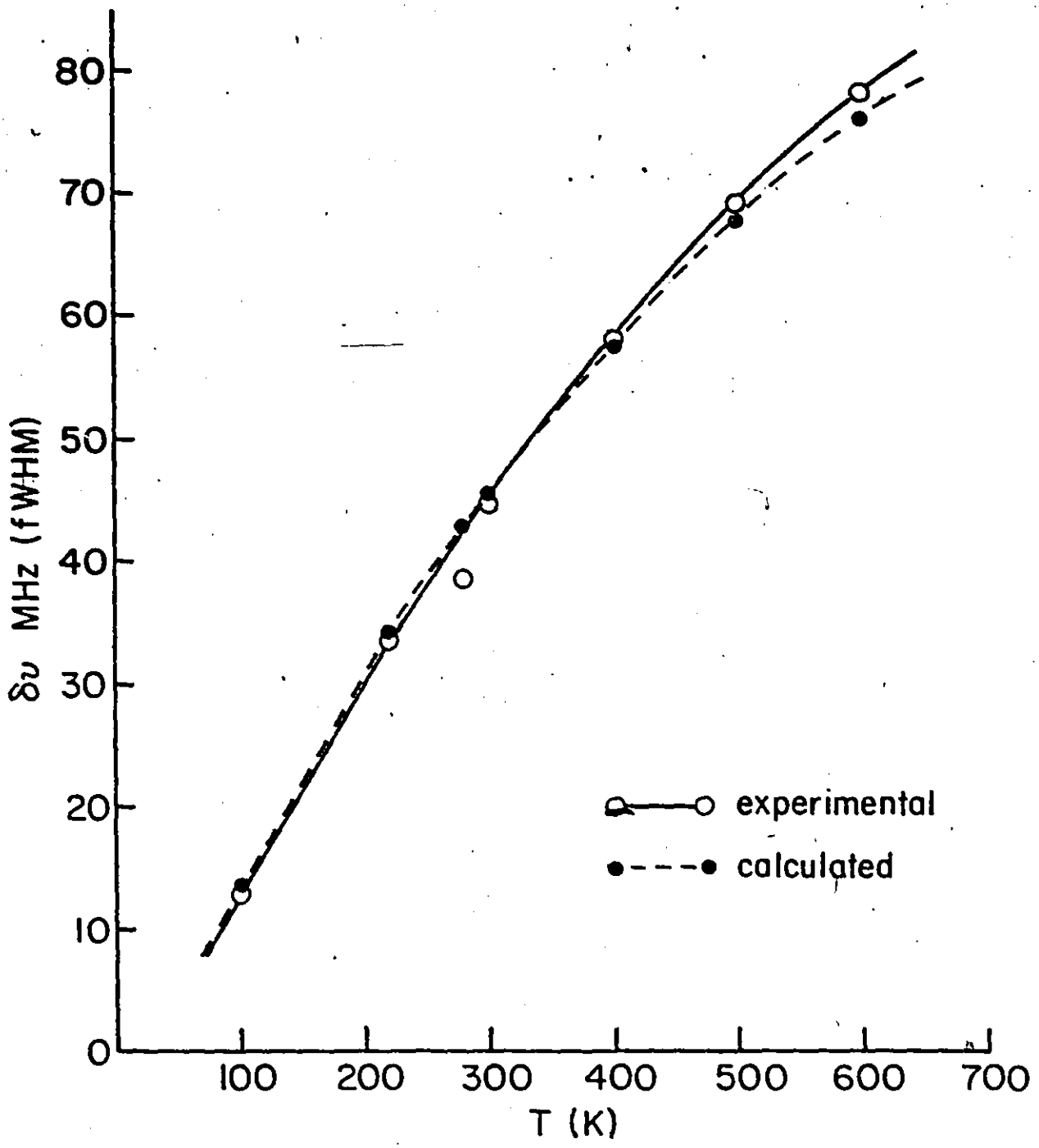
80
70
60
50
40
30
20
10
0
δω MHz (fWHM)
100
200
300
400
500
600
700
T (K)
experimental
calculated

Fig. 3.2

fig. 3.1 is for $\tau = 8.34\times10^{-12}$ sec. The lifetime τ is, of course, a constant for a given temperature.

Using these values, it is observed that the measured values are lower than the calculated values for most of the authors.

From the value of τ at 300°K (as calculated from Fig. 3.1), we can extrapolate the relaxation time above or below 300°K assuming that it depends on temperature as 1/T. In this way the line width of 28 GHz longitudinal acoustic phonon, in α-quartz along the x-axis at various temperatures was evaluated and is shown in fig. III.2. We found that the linewidth calculated in this way is in agreement with Pine's [34] experimental results.

We can also find the lifetime of thermal phonons from the definition of thermal conductivity which is given as in the dominant phonon approximation.

$$K = \frac{1}{3} C_v \bar{v}^2 \tau \qquad \text{(III.4)}$$

where $\bar{v}$ is the average velocity of sound in the medium given by

$$\frac{3}{\bar{v}^3} = \frac{1}{v_\ell^3} + \frac{2}{v_t^3} \qquad \text{(III.5)}$$

where v_ℓ and v_t are longitudinal and transverse velocity of sound in the medium, K at room temperature is 1.55×10^{-2} cal sec^{-1} cm^{-1} K^{-1} as given in reference [45A]. The τ calculated by equation (III.4) is then $\simeq 3.12\times10^{-12}$ sec. which

is roughly one third of the value deduced from the acoustic attenuation. This is not surprising, but it does indicate that the usual practice of using τ deduced from thermal conductivity data is probably unreliable.

APPENDIX I

RESONANT CAVITIES

Cavity designing was one of the important tasks in setting up the apparatus for the experiment. We designed three sets of cavities which resonated at 1.67 GHz, 1.856 GHz and 3.456 GHz respectively.

All the microwave ultrasonic transducers need a high intensity electromagnetic field oscillating at the frequency of the ultrasonic waves to be generated. These fields are normally produced in a microwave resonant cavity. The requirements for generation of high effeciency are that the cavity should have a high Q-factor and that the high field region of the cavity, occupied by the transducer should be as large as possible.

The re-entrant coaxial cavity has been the most widely used type when piezo-electric transducers are employed. Therefore we also designed the re-entrant coaxial cavity as shown in the diagram.

The electric field is confined to a small region of the cavity, if a quarter wavelength cavity is used, thus ensuring a large value of area/volume and the Q-factor can be quite high.

The cavity can be regarded as having an inductance due to the short length of coaxial line which is tuned by the capa-

citance formed between the post and the opposite wall. The resonant free space wavelength of such a cavity is approximately given by Moreno's formula [31a]

$$\lambda_0 = 2\pi \left[\frac{K\ell r_1^2}{2\delta} \log\left(\frac{r_2}{r_1}\right)\right]^{1/2} \qquad (1)$$

where K is the dielectric constant of the medium filling the gap and other symbols are defined in figure AI.1.

The expression for λ_0, as written above, neglects the fringing fields and hence gives a slight overestimate of the resonant frequency. Thus a cavity with ℓ = 3.325 cm, δ = 0.3 cm, r_1 = 0.3 cm and r_2 = 1.9 cm, gives a calculated resonance frequency of 1.73 GHz for quartz where K = 3.8; whereas experimentally this cavity is resonant at about 1.67 GHz. The other two cavities were also resonant at the lower frequencies as compared to the calculated resonance frequencies. Nevertheless, the given equation is quite good for the cavity design. It is often desirable for the resonant cavity to be tenable over a small range and we made it possible in the case of our re-entrant coaxial cavity. In general, this can be achieved in several ways. The value of δ is adjustable as the screw is provided at the back of the post and hence the depth can be adjusted. A similar effect is obtained if the transducer is moved in and out; the effective dielectric constant in the gap then varies and the resonant frequency changes. There is of course, a limit to the extent of the movement of the trans-

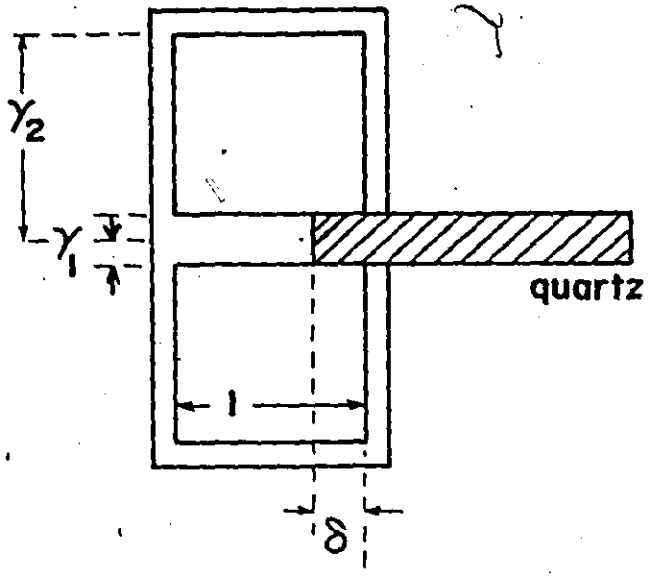

Fig. A1.1

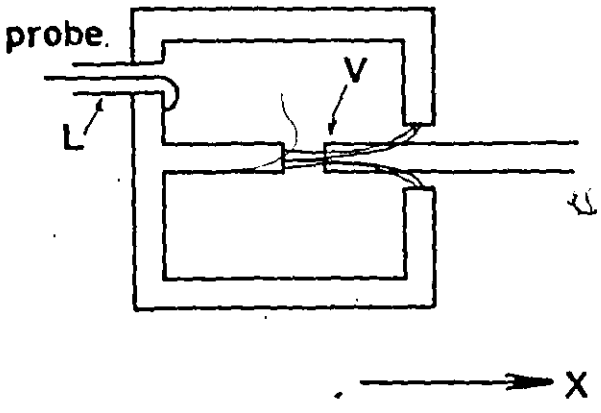

Fig. A1.2

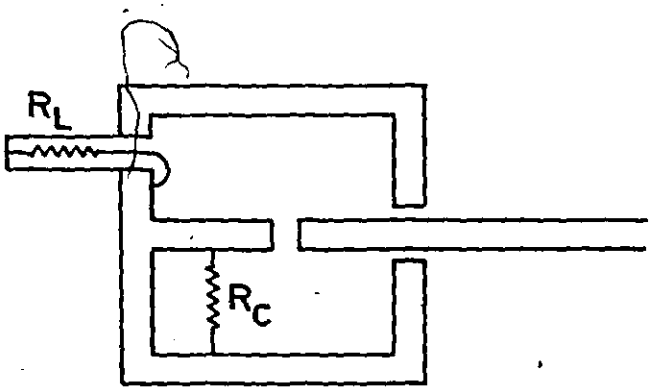

Fig. A1.3

Re-entrant coaxial resonant cavity

ducers; otherwise it will move right out of the electric field of the cavity. We gave consideration to the various other cavity designs but the re-entrant coaxial cavity was the best.

A brief theoretical discussion about the re-entrant coaxial cavity:

Let us examine the excitation process that occurs in the given set of the cavity, as shown in figure AI.2. The arrangement consists of the re-entrant cavity and the piezo-electric quartz rod, with a cross-section, say q, of which only a small volume shall be inside the cavity. The electric field of the cavity is mainly concentrated in the volume V. The rod axis parallel to the crystalline x-axis. The x-component of the field is strongest at the quartz surface: x=0 and decays for larger distances x. As will be evident, the form of this decay is of little importance, and for simplicity we will assume an exponential decay $e^{-\psi x}$. Since the field also oscillates with the resonance frequency $\omega/2\pi$ of the cavity, the x-component of field in the quartz is

$$E = E_0 e^{-\psi x} \cos\omega t. \qquad (2)$$

If a power P is fed into the cavity by means of a matched coaxial lead and if only the x-components of the field are taken into account, the energy density of the field can be expressed by

$$\frac{\varepsilon E_0^2}{8\pi} = \frac{PQ_0}{wV} \qquad (3)$$

where ε is the dielectric constant of quartz, Q_0 being the quality factor of the unloaded cavity and V is the suitably defined "effective" volume of the rod exposed to the electric field. Since the crystal is x-cut - the field causes a piezo-electric stress which in the absence of any strain - is given as

$$X_x^p = d_{11} c_{11} E \qquad (4)$$

where d_{11} and c_{11} are the appropriate piezo-electric and elastic constants. At the free boundary x=0, the total stress X_x must disappear, hence we have a strain

$$X_x = -d_{11} E \ . \qquad (5)$$

Now the simplest solution, satisfying the boundary condition, is a travelling wave of the form

$$X_x = -d_{11} E_0 \cos(\omega t - \frac{2\pi x}{\lambda}) e^{-\alpha x} \qquad (6)$$

where the acoustical wavelength λ and the absorption coefficient α are assumed to be field independent. The energy transferred from the electrical field to such an acoustic wave equals the work done by the strain X_x against the piezo-electric stress X_x^p, and is per period, integrated over the whole crystal. Therefore we can find the incident electrical power converted into acoustical energy. The same treatment can also be applied for the transverse waves. In figure AI.3, R_L and R_C are

resistances representing losses due to the coupling lead and due to dissipation in the cavity respectively.

APPENDIX II

FABRY PEROT INTERFEROMETER

In our set up, the spectrometer used should be able to resolve not only the frequency shifts which lie in the range of 1 to 100 GHz but must also be able to measure the linewidths down to typically a few megahertz. For such a high resolution the Fabry Perot interferometer is the only available instrument.

The Fabry Perots are capable of extremely high spectral resolution, are extremely efficient and are spectrally tunable (transmission typically ranges from 40% to 99%).

A Fabry Perot is constructed with two partially transmitting mirrors which may be flat or radiused, that are parallel to each other. This is said to be a Fabry Perot (FP) cavity. If the cavity is illuminated with a beam of coherent, monochromatic light, it will transmit the beam when the optical path ~~length~~ between the surfaces is an integral number of half, quarter or eighth wavelengths of the incident light. The fractional wavelength varies with the type of cavity used.

In an air-spaced etalon (as in our case) two mirrors or plates as they are often called, are used with partially transmitting coatings on their "first" surfaces and anti-reflection coatings on their "second" surfaces. Normally the second surface is slightly wedged (10 to 30 min.) with respect to first surface to avoid forming additional cavities.

Tuning can be accomplished by moving one mirror with respect to the other - and in our set up, it was done by piezo-electric crystals. Piezo-electric tuning is one of the best methods and allows rapid repetitive tuning.

Fabry Perots typically use 1" to 2" diameter mirrors with flatness of $\lambda/100$ to $\lambda/200$ where plots are normally specified for $\lambda = 5000$ Å. The parallelism and position of two mirrors must be maintained to within $\lambda/100$ to $\lambda/200$ Å for many hours in our case. A FP should have adequate thermal and mechanical stability. And such stability is attained by massive construction, well constrained symmetrical design, use of high linearity piezo-electric drives for remote adjustments and tuning and extensive use of low thermal expansion materials.

The condition for constructive interference for a transmitted wave front is

$$2\eta d\cos\theta = m\lambda \qquad (1)$$

where η is the refractive index of the medium between the two reflecting surfaces; d is the mirror spacing; θ is the inclination of the normal of the mirrors to the wavefront direction; m is the order of interference and λ is the wavelength.

The spectral display obtained with a FP is repetitive. The range of wavelengths which can be displayed in the same spectral order without falling into adjacent orders is termed Free Spectral Range (FRS) = $c/2d$; where c is the velocity of light. And free spectral range (FSR) plays a very important role in the system. The output of the FP for incident light of

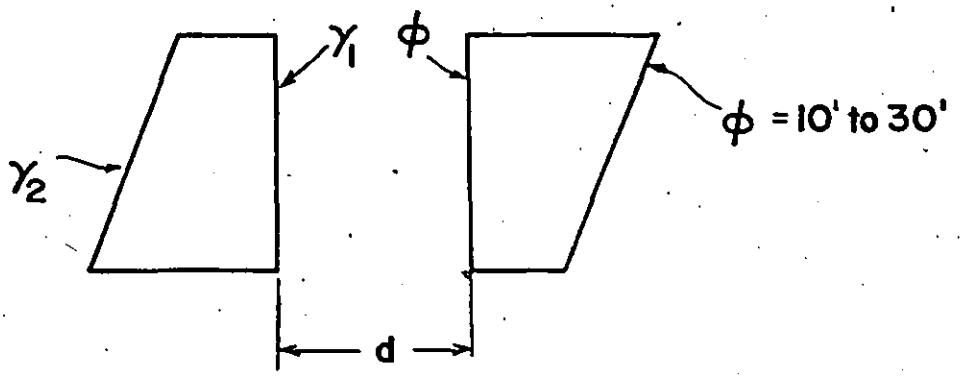

$\gamma_1 = \gamma_2 = \alpha$ plane parallel mirrors

Fig. A2.1

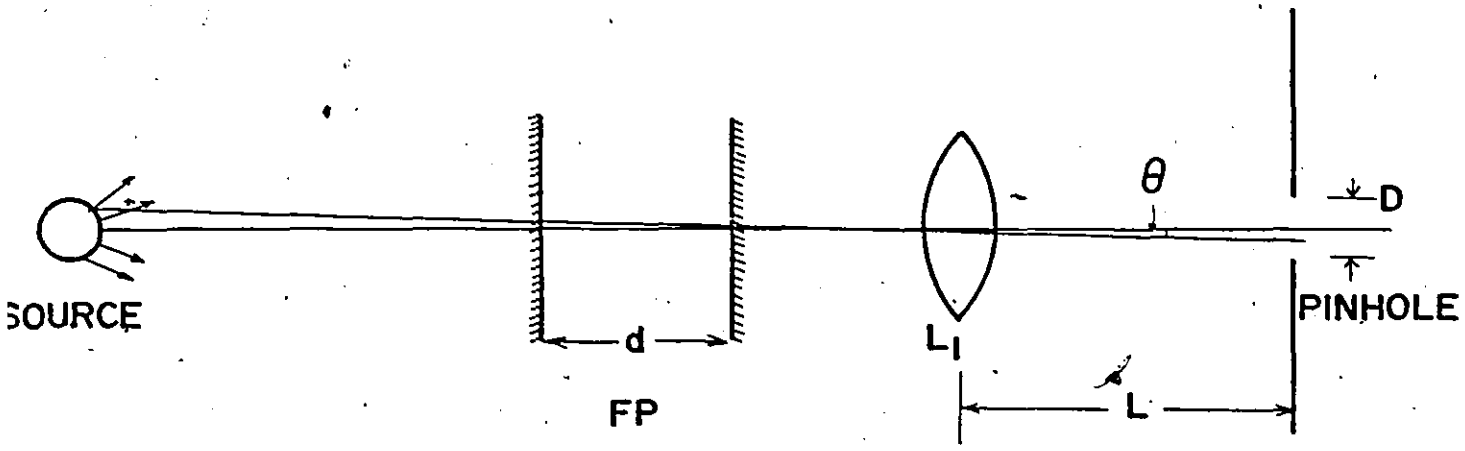

Fig. A2.2

Pinhole finesse

wavelength λ_1 is a series of peaks. The instrument acts as a tunable filter whose peak transmission is close to unity over a narrow spectral interval. Outside the interval the transmission is very low.

The width of the transmission peak determines the resolution of the instrument. The ratio of F.S.R. to width is known as the Finesse (F).

$$F = \frac{FSR}{width} .$$

The F is typically 50 to 100 - in our case, it was in the range of 40-50. The finesse is the key measure of the interferometer's ability to resolve closely spaced lines. The major factors that could limit the net finesse are:

(a) mirror reflectivity of less than unity

(b) lack of parallelism and/or planeness of the mirrors

(c) diffraction losses arising from the finite aperture of the interferometer.

We can define another finesse as reflectivity finesse F_R given by,

$$F_R = \frac{\pi\sqrt{R}}{1-R} . \qquad (2)$$

There is yet another type of finesse, which is defined as Pinhole finesse F_p. If we see figure A2.2, we find the maximum path length change is

$$d - d\cos\theta = \frac{1}{F_p} \frac{\lambda}{2} . \qquad (3)$$

Putting $\cos\theta = 1 - \frac{\theta^2}{2!} + \cdots$ we get

$$F_p = \frac{4\lambda L^2}{D^2 d} \qquad (4)$$

where d is the plate spacing; D is the pinhole diameter as shown in figure A2.2. If f_1 is focal point of lens L_1, then $\theta = \frac{D}{2f_1}$.

Normally F_p should be 2 or 3 times the value of the desired operating finesse; although it may result in some loss of transmission. And also the pinhole must be exactly on axis or the pinhole finesse will be much reduced due to the nonlinear change in fringe radius with angle.

Piezo-electric drive:

Three independent piezo-electric elements were used for alignment by adjusting the voltage to each element separately and for tuning and adjusting the voltage to all three simultaneously. To improve upon contrast and resolution, we changed our single pass system to the triple-pass interferometer.

TRIPLE PASS INTERFEROMETER:

The light is passed through one interferometer three times. Corner cube reflectors were used to return the light parallel to itself as shown in figure A2.3. The triple-pass was about optimum for high contrast with low losses and moderate finesse. The peak transmission was as high as 25% to 40%. The multipass interferometer can be operated up to quite high resolution by increasing the mirror spacing.

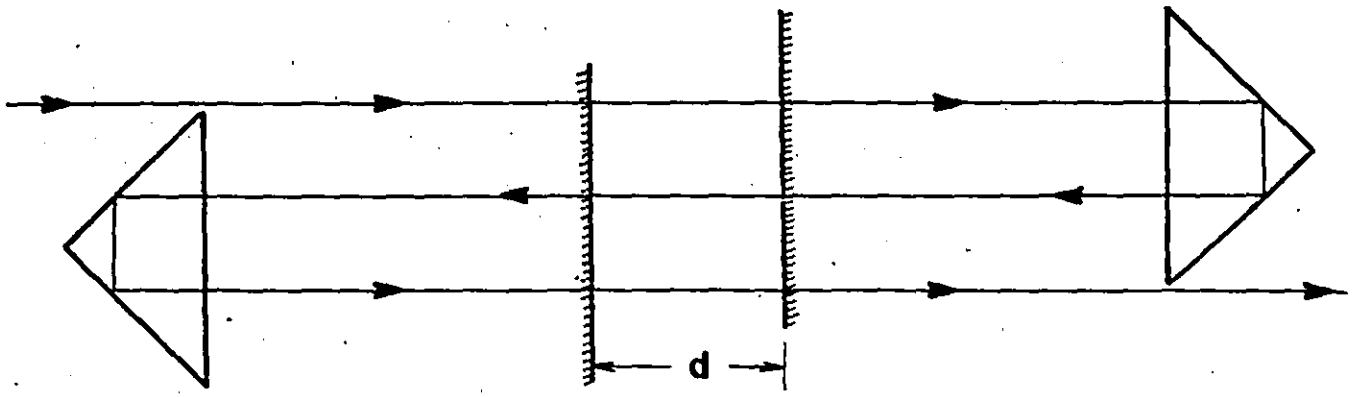

Fig. A2.3
Corner cubes for triple pass FP

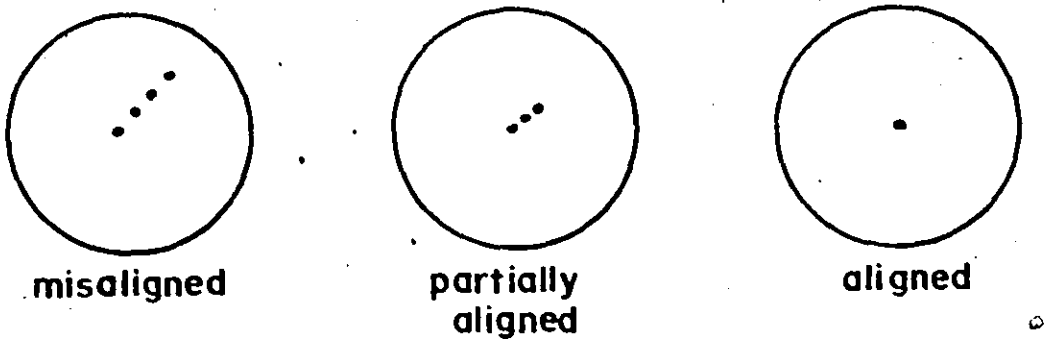

Fig. A2.4

Alignment of FP

How to align a Fabry-Perot interferometer:

There are two requirements for aligning a FP. First the FP must be aligned relative to the incoming radiation. In most cases, FP is normal to the input. The degree of angular alignment required is not great. Reflecting a gas laser reference beam, which is coincident of optical axis, back to itself as well as can be determined visually is normally adequate. The input radiation should be centred on the FP apertures.

Second, the FP plates should be aligned relative to each other. Initial alignment is easiest with a small CW-laser; the wavelength is not important since even 20% to 30% reflectivity is adequate for this step.

When we illuminate the FP with the laser and look at the output on a white card, we observe a train of dots, resulting from reflections on the misaligned plots as shown in figure A2.4. The coarse adjust mechanism should be used to collapse the dots to a single spot. Now the plates will be sufficiently well aligned to see the fringes.

Now if FP is illuminated with a large, collimated monochromatic beam at a wavelength within the spectral range of the plates; a couple of straight line fringes will be observed on a white card. Fine adjust mechanism should be used to adjust for fringes and for even transmission across the aperture when the FP is tuned to the input wavelength.

APPENDIX III

GRÜNEISEN CONSTANT

In an infinite single crystal, it is possible to propagate in any given direction three plane elastic waves with mutually orthogonal displacement vectors. Except for propagation on certain symmetry axis, these waves have different velocities and attenuation coefficient. We know that the ultrasonic attenuation can arise from interactions of ultrasonic wave with

a) thermal phonons
b) free electrons
c) dislocations (This interaction was ruled out by Bömmel et.al. [8])
d) isotopes of different mass from the majority. (This interaction was ruled out by Orbach [32a].)
e) lattice defects and specimen boundaries
f) relaxation and diffusion mechanism involving impurities and other lattice defects
g) paramagnetic impurities
h) spin waves.

Only recently it has been found that the dominant ultrasonic attenuation in good single crystals of dielectric materials is by mechanism (a); and at high temperature, one well known attenuation of type (a) is the thermo-elastic mechanism. As we know, in Akhieser [1] mechanism, the ultrasonic wave causes a separation in the temperature of different groups of thermal

phonons. The subsequent relaxation of this non-equilibrium distribution by phonon-phonon ie Umklapp process results in ultrasonic attenuation.

The third order elastic-constant measurements determine the frequency change of a low frequency ultrasonic wave when propagating in a material subjected to a uniform static stress. The results of these can be used to compute the frequency change of thermal phonons in the crystal when propagating in the stress field of a high frequency ultrasonic wave. Brügger [10] gives a detailed discussion on this aspect of the theory.

The anharmonic properties of solids are generally described in terms of the Grüneisen parameter ν as

$$\nu = \frac{\alpha}{K_T C_v} = \frac{\alpha}{K_s C_p} \qquad (1)$$

with α being the thermal volume expansivity, K_T and K_s the isothermal and isentropic compressibilities and C_p and C_v the isochoric and isobaric capacities. Gamma can also be expressed as the weighted average of generalized parameters ν_i

$$\nu = \frac{\sum_i \nu_i c_i}{\sum_i c_i} \qquad (2)$$

where ν_i expresses the volume dependence of the lattice vibrational frequency for a mode i and c_i being the heat capacity associated with that mode. Now the thermal expansion of rhombohedral or trigonal crystals are fully described by the diagonal elements of the expansivity tensor, therefore according to Brügger and Fritz [12], $\nu_\perp = \nu_{11} = \nu_{22}$ and $\nu_{||} = \nu_{44}$. Therefore

$$\nu = 2\nu_{\perp} + \nu_{||} \tag{3}$$

where $\nu_{\perp} \equiv \nu_{(\text{perpendicular})}$ and $\nu_{||} = \nu_{(\text{parallel})}$. Brügger gives the general formulation in the case of trigonal crystals as

$$\nu = \frac{\sum_p \oint d\Omega\ \Gamma(p,\vec{N})\,\xi(p,\vec{N})}{\sum_p \oint d\Omega\ \xi(p,\vec{N})} \tag{4}$$

$$\nu_{\perp} = \frac{\sum_p \oint d\Omega\ \Gamma_{\perp}(p,\vec{N})\,\xi(p,\vec{N})}{\sum_p \oint d\Omega\ \xi(p,\vec{N})} \tag{5}$$

$$\nu_{||} = \frac{\sum_p \oint d\Omega\ \Gamma_{||}(p,\vec{N})\,\xi(p,\vec{N})}{\sum \oint d\Omega\ \xi(p,\vec{N})} . \tag{6}$$

All the notations used are explained below:-

$$\Gamma(p,\vec{N}) = -\frac{B}{2\omega}\,(1 + 2\omega\rho + r) \tag{7}$$

$$2\Gamma_{\perp}(p,\vec{N}) = -\frac{B}{2\omega}\,[N_1^2 + N_2^2 + 2\omega\rho_{\perp} + r_{\perp}] \tag{8}$$

$$\Gamma_{||}(p,\vec{N}) = -\frac{B}{2\omega}\,[N_3^2 + 2\omega\rho_{||} + r_{||}] \tag{9}$$

where

$$\omega(p,\vec{N}) = c_{11}R_1 + c_{66}R_2 + c_{33}R_3 + c_{44}R_4 + c_{13}R_5 + c_{14}R_6 \tag{10}$$

$$\rho(p) = (S_{11} + S_{12} + S_{13})(U_1^2 + U_2^2) + (2S_{13} + S_{33})U_3^2 \quad (11)$$

$$\rho_{\perp}(p) = (S_{11} + S_{12})(U_1^2 + U_2^2) + 2S_{13}U_3^2 \quad (12)$$

$$\rho_{||}(p) = S_{13}(U_1^2 + U_2^2) + S_{33}U_3^2 \quad (13)$$

also

$$r(p,\vec{N}) = \sum_{i=1}^{6} \tau_i R_i \quad (14)$$

$$r_{\perp}(p,\vec{N}) = \sum_{i=1}^{6} \sigma_i R_i \quad (15)$$

$$r_{||}(p,\vec{N}) = \sum_{i}^{6} \pi_i R_i \quad (16)$$

with

$$R_1(p,\vec{N}) = (N_1U_1+N_2U_2)^2$$

$$R_2(p,\vec{N}) = (N_1U_2-N_2U_1)^2$$

$$R_3(p,\vec{N}) = N_3^2U_3^2$$

$$R_4(p,\vec{N}) = (N_2U_3+N_3U_2)^2 + (N_3U_1+N_1U_3)^2$$

$$R_5(p,\vec{N}) = 2(N_1U_1+N_2U_2)N_3U_3$$

$$R_6(p,\vec{N}) = 2[(N_1^2-N_2^2)U_2U_3+N_2N_3(U_1^2-U_2^2)+2N_1U_1(N_2U_3+N_3U_2)] \quad (17)$$

Also

$$\tau_i = (S_{11}+S_{12}+S_{13})C_i' + (2S_{13}+S_{33})C_i''$$

$$\sigma_i = (S_{11}+S_{12})C_i' + 2S_{13}C_i''$$

$$\pi_i = S_{13}C_i' + S_{33}C_i'' \quad (18)$$

$$c_1' = c_{111} + c_{112} \qquad c_1'' = c_{113}$$
$$c_2' = \tfrac{1}{2}(-c_{112} + c_{222}) \qquad c_2'' = \tfrac{1}{2}(c_{113} - c_{123})$$
$$c_3' = 2c_{133} \qquad c_3'' = c_{333}$$
$$c_4' = c_{144} + c_{155} \qquad c_4'' = c_{344}$$
$$c_5' = c_{113} + c_{123} \qquad c_5'' = c_{133}$$
$$c_6' = c_{114} + c_{124} \qquad c_6'' = c_{134} . \qquad (19)$$

In studying the thermo-elastic properties of crystal, one is directly concerned with only eleven Laue's groups and not with the thirty-two point groups. This results from the fact that thermo-elastic properties are always entrosymmetrical. All point groups belonging to the same Laue group have common arrays of elastic coefficients.

When we substitute plane wave solutions into the equations of motion for anisotropic medium gives the well known relations

$$\rho V^2 U_{mn} = \lambda_{mn} U_n \qquad (20)$$

and

$$\lambda_{mn} = C_{mrns} N_r N_s \qquad (21)$$

where the summation over repeated indices is implied. ρ is the density of the medium and V the wave speed. U and N are unit vectors along the directions of polarization and propagation and hence their components U_m, N_r etc. are direction cosines. The small c's are the second order adiabatic elastic stiffness

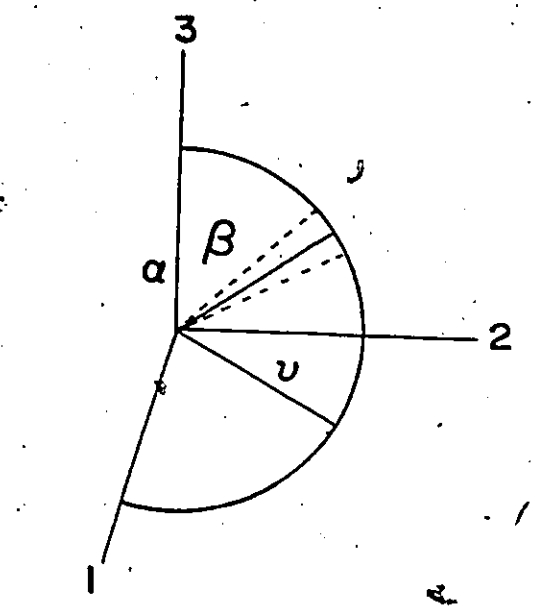

Fig. A3.1

Pure mode directions as given by Brügger

coefficient in tensor notations. Now according to Brügger [10], in the first rhombohedral group RI, the first coordinate axis is diagonal and therefore,

$$N_2N_3[(N_1^2+N_2^2)A-N_3^2C] + [3N_1^2(N_3^2-N_2^2)-N_2^2(3N_3^2-N_2^2)]a = 0 \quad (22)$$

$$N_1N_3[(N_1^2+N_2^2)A-N_3^2C] - N_1N_2[3N_1^2-N_2^2-6N_3^2]a = 0 \quad (23)$$

$$N_1N_3(N_1^2-3N_2^2)a = 0 \quad . \quad (24)$$

The α-direction remains unchanged as in the figure.

$$N_1 = N_2 = 0 \quad ; \quad N_3 = 1 \quad .$$

The β-directions move into the coordinate plane perpendicular to the diagonal axis

$$N_1 = 0 \quad ; \quad N_3/N_2 = k$$

where k satisfies the above equation q with p=0 or

$$k^3 + \frac{3a}{C} k^2 - \frac{A}{C} k - \frac{a}{C} = 0 \quad (25)$$

whereas for the ν-direction

$$N_2/N_1 = \sqrt{3} \quad ; \quad N_3 = 0 \quad .$$

The notations used in the above equations are

$$a = c_{14} \; ; \; a_2 = c_{15} \; ; \; A = c_{11}-2c_{44}-c_{13} \; ; \; C = c_{33}-2c_{44}-c_{13} \quad (26)$$

Now to determine the polarization directions and wave speeds, equation (20) is solved for all mode directions N determined

as above. For the longitudinal mode L, one has simply U = N, for the two transverse modes T' and T", the components of the corresponding polarization vectors U and V can be expressed in terms of the components of N and the angle ν enclosed by V and the vertical plane through N.

$$U_1 = (1-N_3^2)^{-1/2}[-N_1N_3\sin\nu - N_2\cos\nu]$$
$$U_2 = (1-N_3^2)^{-1/2}[-N_2N_3\sin\nu + N_1\cos\nu] \qquad (27)$$
$$U_3 = (1-N_3^2)^{1/2}\sin\nu$$

		U_1	U_2	U_3
RI_α				
$N_1=N_2=0$	L	0	0	1
$N_3=1$	T	$\cos\theta$	$\sin\theta$	0
RI_β				
	L	0	$1/x$	k/x
$N_1=0$	T_1	1	0	0
$N_3/N_2=k$	T_2	0	$-k/x$	$1/x$
RI_ν				
	L	$1/2$	$\sqrt{3}/2$	0
$N_2/N_1=\sqrt{3}$	T_1	$-\frac{1}{2}\sqrt{3}\cos\nu"$	$\frac{1}{2}\cos\nu"$	$\sin\nu"$
$N_3=0$	T_2	$\sqrt{3}/2\ \sin\nu"$	$-\frac{1}{2}\sin\nu"$	$\cos\nu"$

$$N_3/N_2 = k \qquad x = (1+k^2)^{1/2}$$

$$\cot 2\nu'' = \frac{c_{11}-2c_{44}-c_{12}}{4c_{14}} .$$

Thus after substitution, we calculate

$$C_1' = -5.55 \qquad C_2' = 0.065 \qquad C_3' = 6.24$$

$$C_4' = -3.34 \qquad C_5' = -2.82 \qquad C_6' = -1.78 .$$

(All the values are multiplied by 10^{12} dyne/cm^2)

Similarly

$$C_1'' = 0.12 \qquad C_2'' = -1.41 \qquad C_3'' = -0.815$$

$$C_4'' = -1.10 \qquad C_5'' = -3.12 \qquad C_6'' = 0.02$$

(All the values of C"'s are again multiplied by 10^{12} dyne/cm^2 or 10^{11} N/metre^2)

Also elastic compliances S_{ij} are given in 10^{-12} m^{2}N^{-1}

$$S_{11} = 12.77 \qquad S_{12} = -1.79 \qquad S_{44} = 20.04$$

$$S_{14} = 4.50 \qquad S_{33} = 9.60 \qquad S_{66} = 29.12$$

$$S_{13} = -1.22$$

then

$$\tau_i = 9.76\, C_i' + 7.16\, C_i''$$

$$\sigma_i = 10.98\, C_i' - 2.44\, C_i''$$

$$\pi_i = -1.22\, C_i' + 9.60\, C_i'' .$$

Now the values of third order elastic constants are given by McSkimmin et.al. [46]

$C_{111} = -2.10$	$C_{134} = 0.02$
$C_{112} = -3.45$	$C_{144} = -1.34$
$C_{113} = 0.12$	$C_{155} = -2.00$
$C_{114} = -1.63$	$C_{222} = -3.32$
$C_{123} = -2.94$	$C_{333} = -8.15$
$C_{124} = -0.15$	$C_{344} = -1.10$
$C_{133} = -3.12$	$C_{444} = -2.76$.

Again all the values are multiplied by 10^{12} dynes/cm^2. On substituting these values we get

$\tau_1 = -5.33088$	$\tau_2 = 0.94612$
$\tau_3 = -11.92564$	$\tau_4 = -4.04744$
$\tau_5 = -4.98624$	$\tau_6 = -1.72296.$

Similarly

$\sigma_1 = 6.12318$	$\sigma_2 = 0.41541$
$\sigma_3 = -4.86292$	$\sigma_4 = -3.39892$
$\sigma_5 = -2.33508$	$\sigma_6 = -1.95932$

and

$\pi_1 = 0.7923$	$\pi_2 = -1.36153$
$\pi_3 = -7.06272$	$\pi_4 = -0.64852$
$\pi_5 = -2.65116$	$\pi_6 = 0.23636$

We also know the value of elastic stiffness in the units of 10^{11} dynes/cm^2 as given below

$$c_{11} = 8.674 \qquad c_{12} = 0.699$$
$$c_{33} = 10.72 \qquad c_{13} = 1.191$$
$$c_{44} = 5.79 \qquad c_{14} = -1.791 \ .$$

If we deal with only longitudinal case and if we substitute these values in equations (8), (9), (10), (11), (12) and (13), we get the value of $\nu_{\perp}$ and $\nu_{||}$. The value of B used is 3.74×10^9 dynes/cm^2. Therefore combining the two values with the formula $\nu = \nu_{||} + 2\nu_{\perp}$, give us the value of the Grüneisen constant, which is 0.708 for the x-direction and along the z-axis it is -0.351. The calculated values are fairly close to the measured values reported by Lewis [21].

BIBLIOGRAPHY

1. Akhieser,A., 1939, J. of Phys., Vol. 1, No. 4, p. 277.
2. Atanasoff, J.V. and Hart, P.J., 1941, Phys. Rev. Vol. 59, p. 85
3. Anderson, O.L., et al., 1968, Rev. of Geophys. Vol. 6, No. 4, p. 491.
4. Birch, F. and Clark, H., 1940, Amer. J. of Science, Vol. 238, No. 9, p. 613.
5. Brainerd, J.G. et al., 1949, Proceed. of IRE, p. 1378.
6. Bechmann, R., 1958, Phys. Rev., Vol. 110, No. 5, p. 1060.
7. Bömmel, H.E. and Dransfeld, K., 1958, Phys. Rev. Letters, Vol. 1, No. 7, p. 234.
8. Bömmel, H.E. and Dransfeld, K., 1960, Phys. Rev. Vol. 117, No. 5, p. 1245.
9. Branskii, K.N., 1958, Soviet Phys-Doklady, Vol. 2, p.237.
10. Brugger, K., 1964, Phys. Rev., Vol. 133, No. 6A, p.A1611.
11. Brugger, K., 1965, J. of Apl. Phys., Vol. 36, No. 3, p. 759.
12. Brugger, K. and Fritz, T.C., 1967, Phys. Rev. Vol. 157, No. 3, p. 524.
13. Cohen, M.G. and Gordon, E.I., 1965, Bell System Tech. J., April, p. 693.
14. Cohen, M.G. and Gordon, E.I., 1966, Bell System Tech. J., (July-Aug.), p. 945.

15. Fitzgerald, T.M. and Silverman, B.D., 1968, Phys. Stat. Solidi, Vol. 27, p. 473.

16. Ganapol'skii, E.M. and Chernets, A.N., 1967, Soviet Phys. JETP, Vol. 24, p. 255.

17. Jacobson, E.H., "Quantum Electronics", C.H. Townes (Ed.) p. 468, 1960.

18. Kwok, P.C., "Ph.D. Thesis", Phys. Dept., Harvard Univ., 1965.

19. Knapp, W.J., 1943, J. of Am. Ceramic Soc., Vol. 26, No. 2, p. 48.

20. Lewis, M.F. and Patterson, E., 1967, Phys. Rev. Vol. 159, No. 3, p. 703.

21. Lewis, M.F., 1968, J. of Acous.Soc. of Ame., Vol. 44, No. 3, p. 713.

22. Liekens, W., Michiels, L. and Debock, A., 1971, J. Phys. C., Vol. 4, p. 1124.

23. Lamb, J. and Richter, J., 1966, J. of the Acous. Soc. of Ame., p. 1043.

24. Lamb, J., Redmond, M., and Steinshleifer, Z., 1959, Phys. Rev. Letters, Vol. 3, No. 1, p. 28.

25. Landau, L. and Rumer, G., 1937, Physik Z. Soviet Union, Vol. 11, p. 18.

25A. Lord, R.C. and Morrow, J.C., 1957, J. of Chem. Phys., Vol. 26, No. 2, p. 230.

26. Mason, W.P. and Bateman, T.B., 1964, J. of the Acous. Soc. of Ame., Vol. 36, No. 4, p. 644.

27. Mason, W.P. and Bateman, T.B., 1966, J. of the Acous. Soc. of Ame., Vol. 40, No. 4, p. 852.

28. Maris, H.J., 1964, Phil. Mag., Vol. 9, p. 901.

29. Mason, W.P., Crystal Physics of Interaction Processes, p. 125, Chap. 6.

30. Mason, W.P., 1960, J. of the Acous. Soc. of Ame., Vol. 32, No. 4, p. 458.

31. McMahon, D.H., 1967, IEEE Trans. of Sonics and Ultrasonics, Vol. SU-14, No. 3, p. 103.

31A. Moreno, T., 1958, MW Transmission design data (Dover,N.Y.).

32. Nava, R. and Rodriguez, M., 1971, Phys. Rev. B., Vol. 4, No. 12, p. 4512.

32A. Orbach, R., thesis, Univ. of California, 1959.

33. Pine, A.S., 1969, Phys. Rev., Vol. 185, No. 3, p. 1187.

34. Pine, A.S., 1969, Light Scattering Spectra of Solids, p. 581.

35. Pomerantz, M., 1965, Phys. Rev., Vol. 139, No. 2A, p. 501.

36. Purdom, R.C. and Prohofsky, E.W., 1970, Phys. Rev. B, Vol. 2, No. 2, p. 551.

37. Roufosse, M. and Klemens, P.G., 1974, J. of Geophys. Res. Vol. 79, No. 5, p. 703.

38. Rytov, S.M., J. Exptl. Theoret. Phys. (USSR), 1935, Vol. 5, p. 843.

39. Rytov, S.M., Izvest. Akad. Nauk SSR, (1937) Ser. Fiz. 2, p. 223.

40. Stephenson, J.G., 1963, Electronics, p. 43.

41. Stewart, E.S. and Stewart, J.L., J. of the Acous. Soc. of Ame., 1963, Vol. 35, No. 7, p. 975.

42. Soga, N., 1968, J. of Geophys. Res., Vol. 73, No. 2, p. 827.

43. Slack, G.A., 1965, Phys. Rev., Vol. 139, No. 2A, p. 507.

44. Sheard, F.W., 1958, Phys. Rev. Letters, p. 1381.

45. Simons, S., Proc. Phys. Soc., 1964, Vol. 83, p. 749.

45A. Touloukian, Y.S. (Ed.), 1967, Thermophysical Prop. of High Temp. Solid Mat.

46. Thurston, R.N., McSkimin, H.J. and Andreatch, P., Jr., 1966, J. of Apl. Phys., Vol. 37, No. 1, p. 267.

46A. Tucker, J.W. and Rampton, V.W., M.W. Ultrasonics in Solid State Phys., 1972.

47. Woodruff, T.O. and Ehrenreich, H., 1961, Phys. Rev., Vol. 123, No. 5, p. 1553.